Journal of Power Sources 247 (2014) 90–94

Contents lists available at ScienceDirect

Journal of Power Sources

journal homepage: www.elsevier.com/locate/jpowsour

Short communication

Carbon nanotube-wired and oxygen-deficient MoO_3 nanobelts with enhanced lithium-storage capability

Jiangfeng Ni [a,*], Guibin Wang [a], Juan Yang [b], Dongliang Gao [b], Jitao Chen [b], Lijun Gao [a], Yan Li [b,*]

[a] School of Energy, Soochow University, Suzhou 215006, China
[b] Beijing National Laboratory for Molecular Sciences, College of Chemistry and Molecular Engineering, Peking University, Beijing 100871, China

HIGHLIGHTS

- CNT-wired and oxygen-deficient MoO_{3-x}/CNT nanostructure is investigated.
- MoO_{3-x}/CNT is fabricated via hydrothermal synthesis and controlled reduction.
- MoO_{3-x}/CNT exhibits a much improved Li-storage property compared with MoO_3/CNT.
- Formation and recovery of metallic MoO_2 may account for the enhanced performance.

GRAPHICAL ABSTRACT

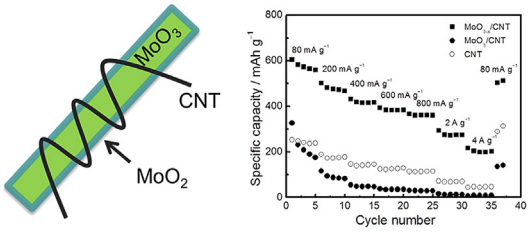

ARTICLE INFO

Article history:
Received 29 June 2013
Received in revised form
12 August 2013
Accepted 19 August 2013
Available online 30 August 2013

Keywords:
Molybdenum oxide
Carbon nanotube
Oxygen deficient
Lithium storage
Conductivity

ABSTRACT

Carbon nanotube (CNT) wired and oxygen-deficient MoO_{3-x}/CNT structures are fabricated via a facile hydrothermal reaction followed by controlled reduction in Ar/H_2. The MoO_{3-x}/CNT, which consists of 63 mol% MoO_3 and 37 mol% MoO_2, exhibits a much improved Li-storage property compared with the original MoO_3/CNT structure when evaluated as an anode in the 0.05–3.0 V region. It is able to retain a capacity of 421 mAh g^{-1} towards Li after 100 cycles at 200 mA g^{-1}, and deliver 293 and 202 mAh g^{-1} at current densities of 2 and 4 A g^{-1}, respectively. It is suggested that the formation and recovery of a metallic MoO_2 phase over the conversion reaction may account for the enhanced performance.

© 2013 Elsevier B.V. All rights reserved.

1. Introduction

Transition metal oxides emerge as a key type of electrode material for energy storage and conversion application in fields such as Li-ion batteries and hybrid supercapacitors [1–4]. Among these materials, molybdenum oxides such as MoO_2 [5–10] and MoO_3 [11–16] have attracted extensive attention due to their high electrochemical activity, suitable lithium reaction voltage, and affordable cost. Particularly, orthorhombic molybdenum trioxide (α-MoO_3) has received a great deal of interests due to the extremely high theoretical Li-storage capacity up to 1117 mAh g^{-1}, based on the full conversion reaction of $MoO_3 + 6Li \leftrightarrow Mo + 3Li_2O$. Moreover, its unique double-layered structure built from MoO_6 octahedron could provide efficient channels for rapid accommodation of

* Corresponding authors. Tel./fax: +86 512 67875503.
E-mail addresses: jeffni@suda.edu.cn, jfengni@gmail.com (J. Ni), yanli@pku.edu.cn (Y. Li).

0378-7753/$ – see front matter © 2013 Elsevier B.V. All rights reserved.
http://dx.doi.org/10.1016/j.jpowsour.2013.08.068

Li ions, thereby manifesting potential for high-power applications such as supercapacitors [11]. However, the utilization of high capacity from MoO_3 anode has principally been hindered by its insulating nature (band gap of 3.1 eV) and structural degradation upon conversion process [13]. To achieve high and stable capacity delivery, the material needs to be engineered to fine particles (5–20 nm) [14] or hierarchical nanostructures [16] to mitigate the above issues. However, scalable fabrication and processing of these nanomaterials remain a significant challenge.

Previously, we demonstrated that CNT-wiring could dramatically improve the stability of MoO_3 cathode upon Li addition reaction (Li_yMoO_3). The CNTs served as efficient electrical wires as well as flexible buffers in the MoO_3/CNT composite [17]. However, this strategy might not work well when MoO_3 is utilized as anode, where conversion dominates the reaction process. Generally, the conversion involves severe particle pulverization and significant volume variation [13]. Due to the nature of point contact, CNT wiring is insufficient to wrap all MoO_3 nanobelts and their degraded fractures, and thus the MoO_3/CNT still suffers from instable cyclability. To circumvent this limitation, here we present a CNT-wiring and oxygen-deficient strategy to realize fully electrical connection of MoO_3 [14]. The oxygen deficiency results in the formation of a metallic MoO_2 phase, which serves as a secondary conductive additive to construct better electrical percolation [10,18]. As a result, this modified MoO_3 electrode shows outstanding cycling efficiency and rate capability.

2. Experimental

Firstly, 20% CNT-wired MoO_3 nanobelts (MoO_3/CNT) were fabricated via a facile hydrothermal approach according to our previous report [17]. Typically, 0.5 g Mo (≥99%) powder was dissolved in 20 ml H_2O_2 (≥30%) solution, and the pH value of the solution was adjusted to ~2 using 6 M HNO_3. Afterward, mildly oxidized CNTs (CNT:MoO_3 = 1:4 by mass) were dispersed in the above solution by sonication. The resultant suspension was then transferred to a 100 ml Teflon-lined stainless steel autoclave and reacted at 180 °C for 12 h. After reaction, the MoO_3/CNT powder was thoroughly washed by deionized water and harvested by vacuum filtration. To prepare oxygen-deficient MoO_{3-x}/CNT, the hydrothermal product was reduced at 400 °C for 2 h in a 5% H_2/Ar flow [5].

The prepared materials were characterized by X-ray diffraction (XRD, Rigaku D/max 2500), scanning electron microscopy (SEM, Hitachi S-4800), transmission electron microscopy (TEM, FEI Tecnai G2 T20), and Raman spectroscopy (LabRAM ARAMIS, Horiba Jobin Yvon). The composition was analyzed by inductively couple plasma (ICP, Varian Vista MPX). X-ray photoelectron spectroscopy (XPS) was carried out on Kratos Axis Ultra spectrometer with Al Kα monochromatized X-ray source.

For electrochemical test, composite electrodes consisting of 85 wt% active material, 10 wt% super-P-Li carbon black, and 5 wt% polyvinylidene fluoride binder were used as work electrode, Li metal as both counter and reference electrodes. The electrolyte was 1 M $LiPF_6$ solution in ethylene carbonate and dimethyl carbonate (1:1 by volume), and the separator was Celgard 2320 porous membrane. 2032-type coin cells were assembled in an Ar-filled glove box (MBraun) with O_2 and H_2O concentration below 0.5 ppm. Galvanostatic charge and discharge tests were performed on a Neware battery test system at room temperature. Electrochemical impedance spectroscopy (EIS) was measured on a Zennium electrochemical workstation (Zahner).

3. Results and discussion

Fig. 1a shows XRD patterns of the MoO_3/CNT and the oxygen-deficient product MoO_{3-x}/CNT. The MoO_3/CNT exhibits a well-

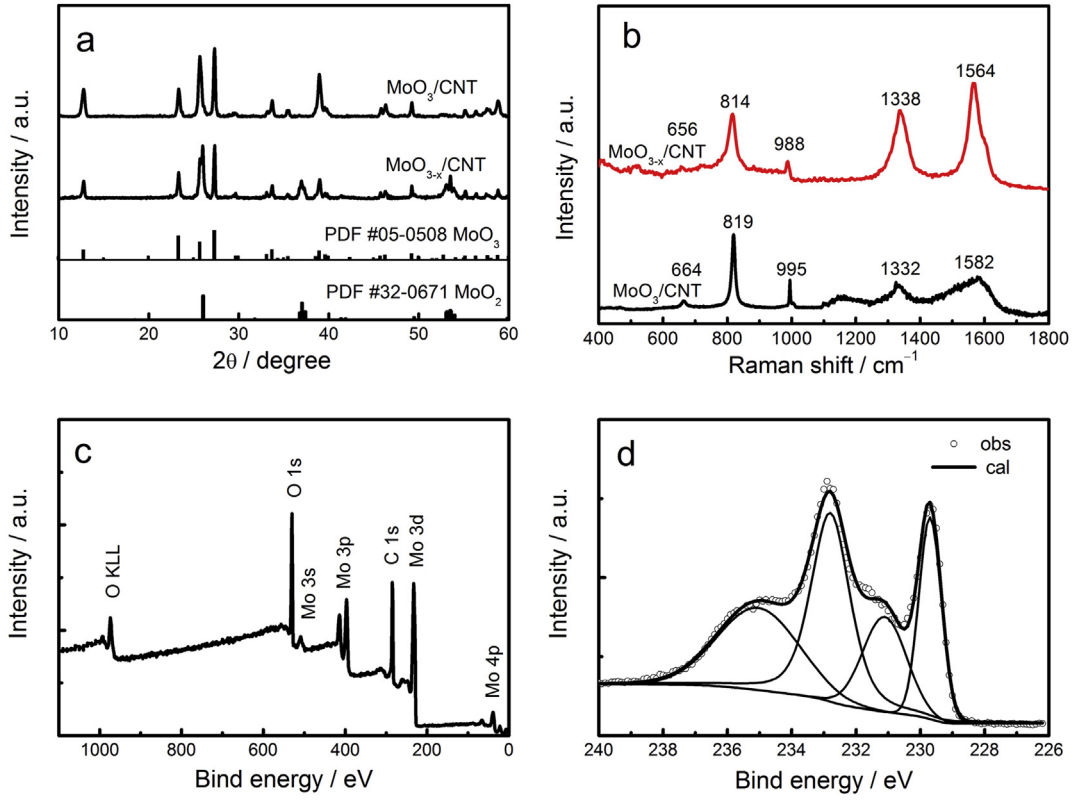

Fig. 1. (a) XRD patterns and (b) Raman spectra of the MoO_{3-x}/CNT and MoO_3/CNT; (c) XPS data of the MoO_{3-x}/CNT; (d) Mo 3d XPS data.

crystallized orthorhombic structure without any impurities (PDF #05-0508). After reduction at 400 °C for 2 h in 5% H_2/Ar atmosphere, two extra peaks at 26.0° and 37.0° are clearly observed, which are characteristic of monoclinic MoO_2 phase (PDF #32-0671). The composition of the MoO_{3-x}/CNT was analyzed by ICP. The result reveals that the MoO_{3-x}/CNT consists of 63 mol% MoO_3 and 37 mol% MoO_2.

Fig. 1b compares Raman spectra of MoO_{3-x}/CNT before and after partial reduction. Clearly, MoO_3 shows three characteristic peaks centered at 995 (Mo═O), 819 (corner-sharing O–Mo–O), and 664 cm^{-1} (edge-sharing O–Mo–O) [17]. All these peaks shift towards low wavenumbers in the spectrum of MoO_{3-x}/CNT, indicating a weaker Mo–O bonding due to oxygen deficiency.

X-ray photoelectron spectroscopy (XPS) showed in Fig. 1c reveals peaks only due to Mo, O and C elements, confirming the presence of CNT and molybdenum oxide. Fig. 1d display the high-resolution spectrum of Mo, which can be mainly deconvoluted into four peaks. Peaks at 229.7 ($3d_{5/2}$) and 232.8 ($3d_{5/2}$) eV with a spin energy separation of 3.1 eV could be due to Mo (IV), while peaks at 231.1 and 235.0 eV can be ascribed to Mo (VI) $3d_{5/2}$ and $3d_{5/2}$, respectively [10]. The ratio of Mo (IV): Mo (IV) was calculated to be 55:45, which is greater than the ICP result. This discrepancy is not unexpected as XPS is a surface-inspection technique while the reductive production most possibly accumulates on the surface of MoO_3 nanobelts.

The materials were further characterized by scanning electron microscopy (SEM) and transmission electron microscopy (TEM) observation. Fig. 2a illustrates a representative SEM image of the MoO_3/CNT, which shows a unique belt-like morphology with high aspects ratio [12,17]. These nanobelts are mostly retained after H_2 reduction, though some are fractured due to cleavage of MoO_3 belts upon H_2 reduction (Fig. 2b). A TEM image shown in Fig. 2c further confirms that the reduced MoO_{3-x} maintains the nanobelt structure, and the CNT network is still well preserved. It should be noted that the reduction of MoO_3 is well controlled in this case, in order to build an efficient conductive surface of MoO_2 while does not disturb the structural integrity of MoO_3 [18]. Thus a good electrical connection of active nanoparticles could be ensured. If the reduction duration of the MoO_3/CNT is extended to 4 h, most MoO_{3-x} nanobelts are cracked and crumbled, and therefore the structural integrity has been destroyed (see Supporting information Fig. S1). Fig. 2d presents the selective area electron diffraction (SAED) on MoO_{3-x}. This diagram contains two sets of diffraction spots that can be indexed to orthorhombic MoO_3 and monoclinic MoO_2, respectively, consistent with XRD pattern [10,12].

The electrochemical Li-storage properties of the MoO_{3-x}/CNT were investigated by CV and galvanostatic tests. Fig. 3a displays the CV profile of the MoO_{3-x}/CNT in the first three cycles. In the initial cycle, two cathodic peaks at 2.63 and 2.17 V (versus Li^+/Li, unless otherwise stated) reflect Li insertion into MoO_3 lattice, while those at 1.55 and 1.26 V represent Li addition into MoO_2 [10]. The significant current peak below 0.5 V can be ascribed to Li conversion reaction where Mo metal and Li_2O are produced [19]. During subsequent cycles, peaks due to Li insertion/extraction in MoO_3 almost disappear, whereas those in MoO_2 well remain, suggesting a better reversibility of MoO_2 versus MoO_3.

Fig. 3b shows the charge and discharge profiles during the first two cycles. The MoO_3/CNT exhibits two voltage plateau at 2.3 and 0.4 V, corresponding to lithium insertion into and conversion with MoO_3, respectively. In the case of MoO_{3-x}/CNT, both 2.3 and 0.4 V plateau are reduced, whereas a slope emerges in the region of 1.5–1.0 V, characteristic of phase transition of the orthorhombic MoO_2 caused by Li insertion [8,10]. Consequently, the MoO_{3-x}/CNT discharges a comparably low initial capacity of 1037 mAh g^{-1} in the range of 0.05–3.0 V. In addition, its following charge capacity of 609 mAh g^{-1} is also significantly below that of the MoO_3/CNT, suggesting that partial Mo is re-oxidized by Li_2O to MoO_2 rather than to MoO_3 [8,10,13]. Recovery of MoO_2 would ensure a better conductivity and thus a better reversibility for the MoO_{3-x}/CNT, as evidenced by almost reproducible charge curves during the initial two cycles.

The evolution of the MoO_{3-x} phase can be identified by post XRD tests (Supporting information Fig. S2). The discharged MoO_{3-x}

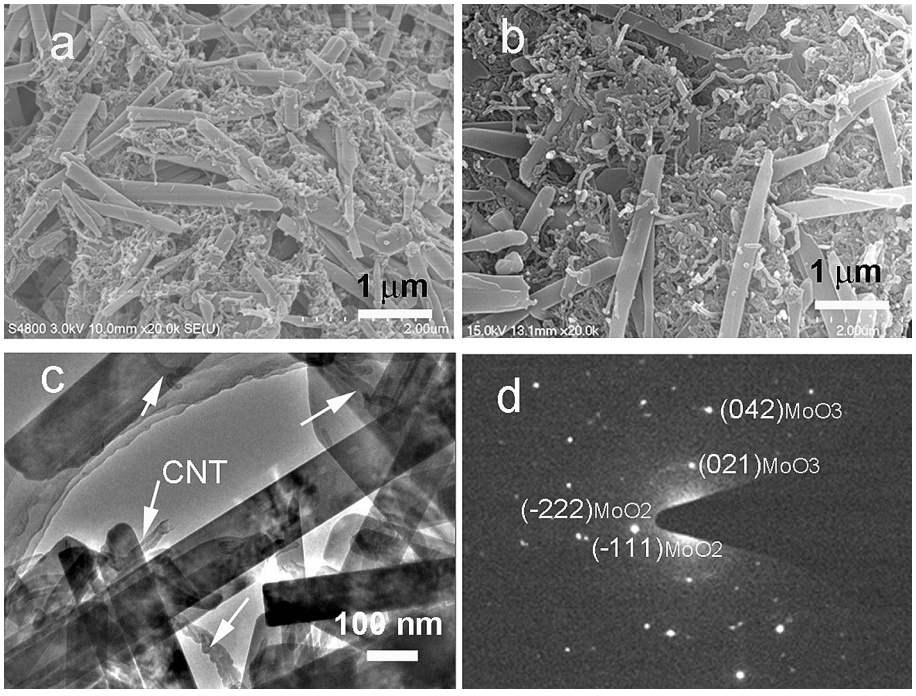

Fig. 2. (a) SEM image of the MoO_3/CNT; (b–d) SEM, TEM and SAED of the MoO_{3-x}/CNT, respectively.

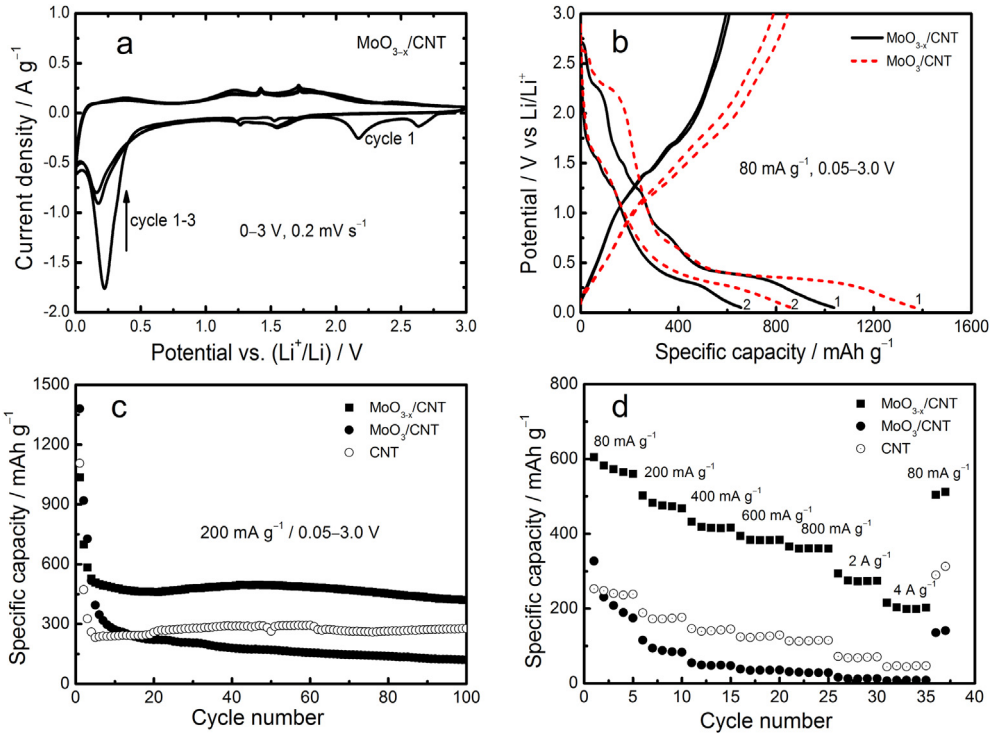

Fig. 3. Electrochemical characterizations of the MoO_{3-x}/CNT and MoO_3/CNT. (a) CV of the MoO_{3-x}/CNT. (b) Galvanostatic profiles for the initial two cycles at 80 mA g^{-1}. (c) Cycling performance at 200 mA g^{-1}. (d) Rate cycling at various current densities.

becomes nearly amorphous with two subtile peaks corresponding to Li_2CO_3, which may be derived from exposure of Li_2O to air. When being recharged, both Li_2MoO_4 (PDF #12-0763) and MoO_2 phases can be detected. The former might be due to partial Li ions trapped in the MoO_3, while the latter suggests that MoO_2 is indeed recovered upon cycling.

Long-term cycle stability of these electrode materials is shown in Fig. 3c. The MoO_{3-x}/CNT exhibits a capacity of 501 mAh g^{-1} at the 6th cycle, and retains 421 mAh g^{-1} after 100 cycles. If the contribution of MoO_{3-x} is distinguished from CNT, which delivers a low capacity of 270 mAh g^{-1}, it would be 470 mAh g^{-1} after 100 cycles. It should be pointed out that only very few works regarding to MoO_3 anode have reported such a long-term cyclability [19]. In contrast, capacity of the MoO_3/CNT rapidly drops to 298 mAh g^{-1} after eight cycles, and then gradually decays to 120 mAh g^{-1} in the 100^{th} cycle.

Apart from the enhanced cycling stability, oxygen deficiency in MoO_{3-x}/CNT also leads to excellent rate capability. As shown in Fig. 3d, the material delivers a capacity of 432 mAh g^{-1} at a charge and discharge rate of 400 mA g^{-1}. At higher rates of 2 and 4 A g^{-1}, it still exhibits capacities of 293 and 202 mAh g^{-1}, respectively. Such a high rate capability is superior to that of the original structure, and outperforms most reports on MoO_3 anode to the best of our knowledge [13–15,20]. The superb high-rate and long-cycle performance of the MoO_{3-x}/CNT proves the effectiveness of the oxygen-deficient and CNT-wired strategy.

In general, MoO_3 electrodes exhibit an instable cycling behavior owing to poor electrical connection and structural degradation during conversion reaction [13]. Although CNT-wiring can modify the connection of MoO_3 belts to conductive network, its effectiveness may be rather limited due to insufficient electrical percolation [21,22]. By introducing a secondary conductive MoO_2 in situ, the electrical percolation of active particles could be substantially improved [23]. Moreover, recovery of partial MoO_2 rather than to MoO_3 upon charge also ensures a good conduction throughout the entire conversion process. Therefore, the MoO_{3-x}/CNT electrode exhibits a great enhancement in cycle and power efficiency for Li-storage. It is also interesting to point out that the reduction of MoO_3 should be controlled to a certain extent. Insufficient (such as 30 min) or too long (such as 4 h) reduction duration both results in products showing poor cyclability (see Supporting information Fig. S3). The former may be due to incomplete percolation of the MoO_2 conductive phase, while the latter may be due to loss of structural integrity of molybdenum oxides.

Fig. 4 shows the electrochemical impedance spectroscopy (EIS) of two electrodes after 5 cycles. Both spectra consist of two semicircles in the high and middle frequencies and a straight line in the low frequency. The semicircle in the high frequency reflects Li ion diffusion across electrode/electrolyte interphase (R_f), while that in the middle frequency is associated with charge transfer reaction (R_{ct}). A simple equivalent circuit is established to interpret the spectra. The fitting results show that the MoO_{3-x}/CNT exhibits a reduced R_f of 5.8 Ω compared with MoO_3/CNT (27 Ω). In addition, the R_{ct} of the former is only 78 Ω versus 129 Ω for the latter, indicating that kinetics over Li diffusion across interphase and the followed charge transfer are indeed facilitated [24].

4. Conclusion

In summary, oxygen-deficient and CNT-wired MoO_3 nanobelts were readily prepared via a facile hydrothermal method followed by H_2 reduction, and their Li-storage behaviors were investigated. In the unique MoO_{3-x}/CNTs structure, the conductive and porous CNTs networks supply efficient scaffold facilitating electron and ion transport, while the MoO_2 phase serves as a secondary conductive additive to ensure fully electrical percolation of active material. Electrochemical test results reveal that the MoO_{3-x}/CNT exhibit remarkably improved cycling stability and rate capability versus

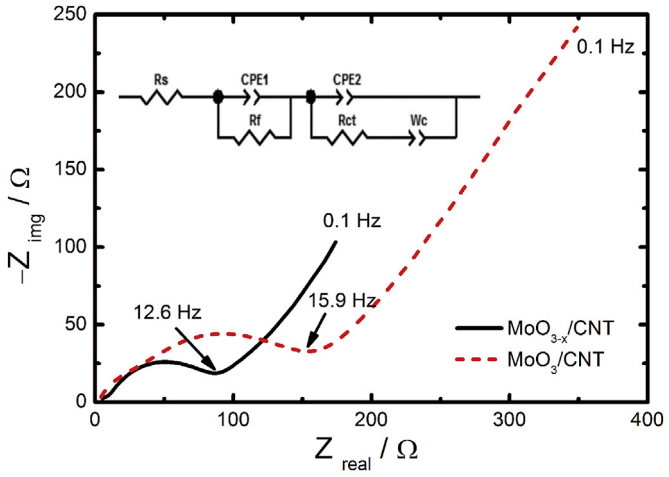

Fig. 4. Impedance spectra of the electrodes after 5 cycles; the inset shows an equivalent circuit for fitting, where R_s represents the solution resistance, R_f the film resistant, R_{ct} the charge transfer resistance, CPE1 and CPE2 the constant phase elements, and W_c the Warburg impedance.

the original composites. It should be noted that this work has only dealt with the conductivity issue of the MoO_3 material; material design by engineering one-dimensional or ultrathin structures of molybdenum oxides might further enhance the rate and cycling performance, and thus imposes a bright future for their potential application [25,26].

Acknowledgments

Support of 863 Program (projects 2009AA035200, 2011AA11A235), NSFC (Projects 21005004, 21125103, 11179011), MOST (Project 2011CB933003) and SRF for ROCS, SEM are gratefully acknowledged. We also thank Lu Chen for the assistance with XRD test.

Appendix A. Supplementary data

Supplementary data related to this article can be found at http://dx.doi.org/10.1016/j.jpowsour.2013.08.068.

References

[1] H. Wang, D. Ma, X. Huang, Y. Huang, X. Zhang, Sci. Rep.2 701 (2012) 1–8.
[2] L. Mai, F. Yang, Y. Zhao, X. Xu, L. Xu, B. Hu, Y. Luo, H. Liu, Mater. Today 14 (2011) 346.
[3] Y.W. Cheng, S.T. Lu, H.B. Zhang, C.V. Varanasi, J. Liu, Nano Lett. 12 (2012) 4206.
[4] Y.-G. Guo, J.-S. Hu, L.-J. Wan, Adv. Mater. 20 (2008) 2878.
[5] J. Zhou, N.S. Xu, S.Z. Deng, J. Chen, J.C. She, Z.L. Wang, Adv. Mater. 15 (2003) 1835.
[6] X. Zhao, M. Cao, B. Liu, Y. Tian, C. Hu, J. Mater. Chem. 22 (2012) 13334.
[7] C. Avendaño, A. Briceño, F.J. Méndez, J.L. Brito, G. González, E. Cañizales, R. Atencio, P. Dieudonné, Dalton Trans. 42 (2013) 2822.
[8] L. Zhou, H.B. Wu, Z. Wang, X.W. Lou, ACS Appl. Mater. Interfaces 3 (2010) 4853.
[9] X. Li, J. Shao, J. Li, L. Zhang, Q. Qu, H. Zheng, J. Power Sources 237 (2013) 80.
[10] Y. Sun, X. Hu, W. Luo, Y. Huang, ACS Nano 5 (2011) 7100.
[11] T. Brezesinski, J. Wang, S.H. Tolbert, B. Dunn, Nat. Mater. 9 (2010) 146.
[12] L. Zhou, L. Yang, P. Yuan, J. Zou, Y. Wu, C. Yu, J. Phys. Chem. C 114 (2010) 21868.
[13] Y.S. Jung, S. Lee, D. Ahn, A.C. Dillon, S.-H. Lee, J. Power Sources 188 (2009) 286.
[14] L.A. Riley, S.-H. Lee, L. Gedvilias, A.C. Dillon, J. Power Sources 195 (2010) 588.
[15] P. Meduri, E. Clark, J.H. Kim, E. Dayalan, G.U. Sumanasekera, M.K. Sunkara, Nano Lett. 12 (2012) 1784.
[16] Shakir, M. Shahid, S. Cherevko, C.-H. Chung, D.J. Kang, Electrochim. Acta 58 (2011) 76.
[17] G. Wang, J. Ni, H. Wang, L. Gao, J. Mater. Chem. A 1 (2013) 4112.
[18] B. Hu, L. Mai, W. Chen, F. Yang, ACS Nano 3 (2009) 478.
[19] N.A. Chernova, M. Roppolo, A.C. Dillon, M.S. Whittingham, J. Mater. Chem. 19 (2009) 2526.
[20] Z. Wang, S. Madhavi, X.W. Lou, J. Phys. Chem. C 116 (2012) 12508.
[21] Y. Hou, Y.W. Cheng, T. Hobson, J. Liu, Nano Lett. 10 (2010) 2727.
[22] J. Ni, L. Gao, L. Lu, J. Power Sources 221 (2013) 35.
[23] Y.-S. Hu, Y.-G. Guo, R. Dominko, M. Gaberscek, J. Jamnik, J. Maier, Adv. Mater. 19 (2007) 1963.
[24] J. Ni, H. Wang, L. Gao, L. Lu, Electrochim. Acta 70 (2012) 349.
[25] Y. Kadoma, T. Akahira, T. Fukuda, K. Ui, N. Kumagai, Funct. Mater. Lett. 5 (2012) 1250004.
[26] J. Yang, Z. Li, J. Wang, Q. Xiao, G. Lei, X. Zhou, Funct. Mater. Lett. 5 (2012) 1250019.